第 30 卷第 1 期
2014 年 1 月

无 机 化 学 学 报
CHINESE JOURNAL OF INORGANIC CHEMISTRY

Vol.30 No.1
192-203

六例 2-氟异烟酸稀土配位聚合物的合成、晶体结构及其荧光和磁学性质研究

王新苗　吴威平　蒋亚辉　杨国平　奚正平*

(教育部合成与天然功能分子化学重点实验室,陕西省物理无机重点实验室,
西北大学化学与材料科学学院,西安　710069)

摘要：首次利用 2-氟异烟酸为配体合成并表征了 6 例一维螺旋链稀土离子配位聚合物,分别为:{[Ln(FINA)$_3$(H$_2$O)$_2$]·H$_2$O}$_n$ (Ln=Pr (**1**), Nd (**2**), Eu (**3**), Gd (**4**)), {[Dy(FINA)$_3$(H$_2$O)$_2$]}$_n$ (**5**)和{[Gd(FINA)$_2$(phen)(OH)]}$_n$ (**6**)(HFINA=2-氟异烟酸,phen=1,10-邻菲罗啉),其中 **1~4** 为相同构型。由于镧系收缩效应的影响,配体在 **1~5** 中表现出不同的配位模式而稀土离子也呈现不同的配位构型。这些一维链通过分子间强的 O–H…O/N 氢键和芳环间的 $\pi\cdots\pi$ 作用以及 C–H…F 氢键等丰富的分子间力连接成三维超分子结构。有趣的是在化合物 **1~4** 中存在可以容纳一个水分子的一维溶剂分子孔道。荧光测试表明:配合物 **3** 表现出铕离子的特征红色荧光,荧光寿命为 333.81 μs;而 4 则表现出配体特征的荧光。变温磁化率测试表明在 **2~6** 中稀土离子间表现为弱的反铁磁相互作用。热重分析表明所合成的配合物均有较好的热稳定性。

关键词：稀土配位聚合物；2-氟异烟酸；螺旋链；荧光；磁性
中图分类号：O614.33；O641.4　　**文献标识码**：A　　**文章编号**：1001-4861(2014)01-0192-12
DOI:10.11862/CJIC.2014.086

Six Lanthanide-Coordination Polymers Based on 2-Fluoroisonicotinic Acid: Synthesis, Structure, Luminescence and Magnetic Properties

WANG Xin-Miao　WU Wei-Ping　JIANG Ya-Hui　YANG Guo-Ping　XI Zheng-Ping*

(*Key Laboratory of Synthetic and Natural Functional Molecule Chemistry of the Ministry of Education, Shaanxi Key Laboratory of Physico-Inorganic Chemistry, College of Chemistry & Materials Science, Northwest University, Xi'an* 710069, *China*)

Abatract: Six new 1D lanthanide-based coordination polymer helical chains with formulas of {[Ln(FINA)$_3$(H$_2$O)$_2$]·H$_2$O}$_n$ (Ln=Pr (**1**), Nd (**2**), Eu (**3**), Gd (**4**)), {[Dy(FINA)$_3$(H$_2$O)$_2$]}$_n$ (**5**), and {[Gd(FINA)$_2$(phen)(OH)]}$_n$ (**6**) (HFINA=2-Fluoroisonicotinic acid, phen=1,10-phenthroline), were synthesized and structurally characterized. It is the first time that 2-Fluoroisonicotinic acid is employed in producing coordination polymers. Carboxylate moieties of the ligand in these compounds exhibit two types of coordination modes because of the lanthanide contraction effect. Ln^{3+} ion is coordinated by eight donor atoms in a distorted bicapped trigonal-prismatic arrangement in **1~4** while in distorted dodecahedron geometry in **5~6**. All of helical chains are further extended via the intermolecular $\pi\cdots\pi$ interactions, strong O–H…O/N hydrogen bonds and C–H…F hydrogen bonds into a 3D supramolecular structures. Interestingly, in **1~4**, there is a small 1D solvent channel along the *b*-axis, where water molecules are located. The luminescence properties of **3** and **4** have been investigated and the result indicate that compound **3** displays intense red luminescence and exhibits the characteristic transition of the Eu^{3+} ion with a decay lifetime of 333.81 μs, while **4** would be attributed to the intraligand fluorescence, based on the emission spectrum of the free ligand. The magnetic properties of **2~6** reveal the weak antiferromagnetic characters. Additionally, the

收稿日期:2013-11-13。收修改稿日期:2013-11-22。
国家自然科学基金(No.21371142,20931005,91022004,21201139);陕西省自然科学基金(No.2013JQ2016)资助项目。
*通讯联系人。E-mail:xizp@c-nin.com

thermal analyses suggest the high thermal stability of compounds **1**~**6**. CCDC: 977317, **1**; 977318, **2**; 977319, **3**; 977320, **4**; 977321, **5**; 977322, **6**.

Key words: lanthanide-coordination polymers; 2-fluoroisonicotinic acid; helical chains; luminescence; magnetism

0 Introduction

Coordination polymers (CPs) and metal-organic frameworks (MOFs) continue to attract much attention[1], because of their intriguing architectures and diversity of functions. In recent years, the design and construction of lanthanide-based coordination polymers (LnCPs) have had an upsurge of interest in these fields, owing to unique optical preferences of lanthanide materials, their intense, line-like, and long-lived emissions, which cover a spectral range from the ultraviolet to the visible and even the near-infrared (NIR) region[2-4]. Furthermore, they have fascinating magnetic behavior such as a large paramagnetism, significant magnetic anisotropy and slow magnetic relaxation[5]. The unique electronic structures of the lanthanide ions make them to be highly promising molecules for the development of unique single molecule magnets (SMMs), 1D magnetic chains like single-chain magnets (SCM), and 2D magnetic layers. For example, a number of Dy(III)-based multinuclear SMMs with slow magnetic relaxation have been described[6].

Although the lanthanide ions are favorable in producing fluorescent and magnetic materials for their intrinsic nature under the influence of the 4*f* electrons, proper organic ligands are crucial in the formation of multifunctional LnCPs. The *f*-*f* transitions of the lanthanides are parity forbidden and direct lanthanide excitation is limited, which make their absorption coefficients extremely small. Therefore, organic ligands with conjugated motifs functioning as chromophores are introduced into the LnCPs to absorb light and transfer energy to the lanthanide ions, it is well known as the "antenna effect", playing an important role in the improvement of the emission efficiency[7-10]. On the other hand, the organic linkers play a crucial role in the exchange magnetic interactions among the neighboring magnetic carriers because magnetism is a cooperative phenomenon. Aromatic carboxylate anions, which have a rigid organic skeleton and strong coordination ability toward many metals, provide both an "antenna" to luminescence and short bridges to magnetism, and therefore they have been proved to be favorable ligands to construct luminescent and magnetic LnCPs[7]. Herein we select 2-Fluoroisonicotinic acid (HFINA) as the ligand based on the following consideration. Firstly, fluorinated (F, CF_3) groups are of great interest to both MOFs and supramolecular networks for they may readily adjust the resulting coordination arrays, the host organizations, and the possible included cavities[11-14]. Furthermore, the fluorinated aromatic groups therein may influence the properties of the resulting complexes such as the thermal and air stability; superacidity; optical and electrical properties based on reported fluorous materials[15-21]. Lastly, the ligand has been not research until now, as far as we know, although its precursor isonicotinic acid has been widely studied. In order to pursuit of multifunctional materials of lanthanide cation and better understand the thermal behavior, luminescence, and magnetic properties of the ligand systems, six new 1D helix lanthanide coordination polymer chains based on 2-Fluoroisonicotinic acid have been synthesized and characterized systematically.

1 Experimental

1.1 Materials and physical techniques

All reagents and solvents employed were commercially available and used as received without further purification. Elemental analyses (C, H, and N) were performed on a Perkin-Elmer 240C element analyzer. Infrared spectra on KBr pellets were recorded on Bruker EQUINOX-55 FT-IR spectrophotometer in the range of 4 000~400 cm^{-1}. Thermal analyses were performed on a NETZSCH STA 449C

microanalyzer with a heating rate of 10 ℃·min^{-1} under N_2 atmosphere. Luminescence spectra for the solid samples were investigated with a Hitachi F-4500 fluorescence spectrophotometer and the luminescent lifetimes were taken on an Edinburgh Analytical Instrument FLsp920. The powder X-ray diffraction (PXRD) patterns were measured using a Bruker D8 advance powder diffractometer at 40 kV and 40 mA for Cu $K\alpha$ radiation (λ=0.154 18 nm), with a scan speed of 0.2 s per step and a step size of 0.02° (2θ). Magnetic data were obtained using a Quantum Design MPMS SQUID 7S magnetometer at an applied field of 1 000 Oe using multicrystalline samples of **2~6** in the temperature range of 1.9 ~300 K. The magnetic susceptibilities were corrected using Pascal′s constant and the diamagnetism of the holder.

1.2 Syntheses of the polymers 1~6

$\{[Pr(FINA)_3(H_2O)_2]\cdot H_2O\}_n$ (**1**) 10 mL aqueous solution of $Pr(NO_3)_3\cdot 6H_2O$ (0.435 0 g, 1 mmol) was added to 50 mL aqueous solution of HFINA (0.423 3 g, 3 mmol) (the pH was adjusted to about 7 with a 1 mol·L^{-1} NaOH solution). The mixture was stirred for 15 min in air and then filtered. The resulting solution was allowed to stand at room temperature for 1 week to produce well-shaped green crystals of **1**. Yield: 0.547 6 g (89% based on lanthanide element). Elemental Analysis(%) Calcd. for **1**, $C_{18}H_{15}N_3O_9F_3Pr$: C, 35.14; H, 2.46; N, 6.83. Found: C, 35.20; H, 2.43; N, 6.79. IR (KBr pellet, cm^{-1}): 3 645m, 3 441br, 1 668m, 1 594s, 1 559s, 1 481w, 1 416vs, 1 288w, 1 263w, 1 235m, 1 097 w, 1 003w, 938s, 900s, 865w, 806m, 781s, 730w, 682 s,599w, 565m, 427w.

$\{[Nd(FINA)_3(H_2O)_2]\cdot H_2O\}_n$ (**2**) Polymer **2** was obtained by the same procedure as **1**, except that $Nd(NO_3)_3\cdot 6H_2O$ was employed, instead of $Pr(NO_3)_3\cdot 6H_2O$. Pink block crystals of **2** were obtained. Yield: 0.538 2 g (87%). Elemental Analysis (%) Calcd. for $C_{18}H_{15}N_3O_9F_3Nd$: C, 34.95; H, 2.44; N, 6.79. Found: C, 35.01; H, 2.43; N, 6.82. IR (KBr pellet, cm^{-1}): 3 645 m, 3 449br, 3 093m, 1 672m, 1 594vs, 1 560vs, 1 461 m, 1 417vs, 1 288m, 1 263s, 1 235s, 1 097m, 1003w, 938s, 900m, 865w, 806s, 781s, 730w, 682s, 600m, 565m, 446w, 428w.

$\{[Eu(FINA)_3(H_2O)_2]\cdot H_2O\}_n$ (**3**) Polymer **3** was obtained by the same procedure as **1**, except that $Eu(NO_3)_3\cdot 6H_2O$ was employed, instead of $Pr(NO_3)_3\cdot 6H_2O$. Colorless block crystals of **3** were obtained. Yield: 0.563 7 g (90%). Elemental Analysis(%) Calcd. for $C_{18}H_{15}N_3O_9F_3Eu$: C, 34.52; H, 2.41; N, 6.71. Found: C, 34.55; H, 2.39; N, 6.74. IR (KBr pellet, cm^{-1}): 3 386br, 3 077s, 1 660s, 1 594vs, 1 556vs, 1 481s, 1 426vs, 1 295m, 1 267m, 1 234s, 1 201s, 1 000m, 943s, 904s, 862w, 819s, 781s, 734w, 688s.

$\{[Gd(FINA)_3(H_2O)_2]\cdot H_2O\}_n$ (**4**) Polymer **4** was obtained by the same procedure as 1, except that $Gd(NO_3)_3\cdot 6H_2O$ was employed, instead of $Pr(NO_3)_3\cdot 6H_2O$. Colorless block crystals of **4** were obtained. Yield: 0.568 4 g (90%). Elemental Analysis (%) Calcd. for $C_{18}H_{15}N_3O_9F_3Gd$: C, 34.23; H, 2.39; N, 6.65. Found: C, 34.25; H, 2.41; N, 6.64. IR (KBr pellet, cm^{-1}): 3 728 w, 3 647m, 3 444br, 1 681m, 1 598s, 1 561vs, 1 480m, 1418vs, 1288w, 1263w, 1235s, 1097w, 939s, 900m, 865w, 807m, 780s, 729w, 683m, 561m, 446w, 421w.

$\{[Dy(FINA)_3(H_2O)_2]\}_n$ (**5**) Polymer **5** was obtained by the same procedure as **1**, except that $Dy(NO_3)_3\cdot 6H_2O$ was employed, instead of $Pr(NO_3)_3\cdot 6H_2O$. Colorless block crystals of **3** were obtained. Yield: 0.470 3 g (76%). Elemental Analysis (%) Calcd. for $C_{18}H_{13}N_3O_8F_3Dy$: C, 34.94; H, 2.12; N, 6.79. Found: C, 34.90; H, 2.21; N, 6.84. IR (KBr pellet, cm^{-1}): 3 416br, 3 078m, 1 594 vs, 1 556vs, 1 484m, 1 428vs, 1 399s, 1 296w, 1 267 w, 1 237s, 1 119w, 1 096w, 1 002w, 945m, 908w, 861w, 814s, 784s, 733w, 684m, 595w, 560w, 532w, 422w.

$\{[Gd(FINA)_2(phen)(OH)]\}_n$ (**6**) In a beaker, 1 mol·L^{-1} aqueous NaOH was added to a solution of 136.1 mg (0.6 mmol) of HFINA in 5 mL of deionized water, until the solution was adjusted to pH≈7.0. 263.4 mg (0.2 mmol) of $Gd(NO_3)_3\cdot 6H_2O$ in 2 mL of deionized water and 263.4 mg (0.2 mmol) of 1,10-phenthroline in 2 mL of CH_3CH_2OH were added successively, and the mixture was stirred for 15 min in air. The mixture was placed into a 25 mL Teflon-lined autoclave under autogenous pressure and heated at 140 ℃ for 72 h, and then the autoclave was cooled over a period of 24 h at a rate 5 ℃·h^{-1}. After filtration, the product was

washed with distilled water and then dried. Colorless crystals of **6** were obtained. Yield: 0.389 8 g (63% based on lanthanide element). Elemental Analysis (%) Calcd. for $C_{24}H_{15}N_4O_5F_2Gd$: C, 45.42; H, 2.38; N, 8.83. Found: C, 45.52; H, 2.41; N, 8.79. IR (KBr pellet, cm^{-1}): 3 405br, 3 072w, 1 671s, 1 605vs, 1 558s, 1 514m, 1 482 w, 1 415vs, 1 288w, 1 261w, 1 230s, 1 143w, 1 101m, 992 w, 936m, 889w, 842m, 804m, 779s, 725s, 674s, 636w, 563w, 530w, 422w.

1.3 Single crystal structure determination

Data were collected at room temperature with a Bruker Apex Ⅱ Image Plate single-crystal diffractometer with graphite-monochromated Mo $K\alpha$ radiation source (λ=0.071 073 nm) operating at 50 kV and 30 mA in ω scan mode for **1~6**. A multi-scan absorption correction was applied with the use of SADABS. The structures were solved by direct methods using the SIR92 program[22] or SHELXS-97[23], and then refined with full matrix least-square methods based on F^2 (SHELXL-97 or SHELX-2013[24]) within the WINGX program[25]. All non-hydrogen atoms were refined anisotropically using the SHELXL program[23]. The hydrogen atoms of the water molecules were located in a difference Fourier map, and the other hydrogen atoms were generated geometrically. In compound **5**, the F atom from the ligand is disordered by symmetry over two sites with occupancies 0.5∶0.5, which has been reported before[26-27]. The detailed crystallographic data and structure refinement parameters for **1~6** are summarized in Table 1. Selected bond lengths of **1~6** are listed in Table 2.

CCDC: 977317, **1**; 977318, **2**; 977319, **3**; 977320, **4**; 977321, **5**; 977322, **6**.

2 Results and discussion

2.1 Description of crystal structures

Crystal structure of **1~4**: Compounds **1~4** are obtained using the same method and single-crystal X-ray diffraction analyses reveal they are isostructural and all crystallize in the monoclinic crystal system, *C*2/*c* space group. So compound **4** is selected as an example to describe the structure. The asymmetric unit of **4** consists of one Gd^{3+} cation, three $FINA^-$ ligands, two coordinated and one lattice water molecules, as depicted in Fig.1. The Gd center is eight-coordinated and the coordination geometry of Gd

Table 1　Crystallographic data and structural refinements for 1~6

Compound	1	2	3	4	5	6
Formula	$C_{18}H_{15}N_3O_9F_3Pr$	$C_{18}H_{15}N_3O_9F_3Nd$	$C_{18}H_{15}N_3O_9F_3Eu$	$C_{18}H_{15}N_3O_9F_3Gd$	$C_{18}H_{13}N_3O_8F_3Dy$	$C_{24}H_{15}N_4O_5F_2Gd$
Formula weight	615.23	618.56	626.29	631.57	618.81	634.65
Crystal system	Monoclinic	Monoclinic	Monoclinic	Monoclinic	Monoclinic	Triclinic
Space group	*C*2/*c*	*C*2/*c*	*C*2/*c*	*C*2/*c*	*C*2/*c*	$P\bar{1}$
a / nm	2.587 4(5)	2.577 9(4)	2.613 3(14)	2.575 1(3)	2.039 7(5)	0.778 63(17)
b / nm	0.960 99(19)	0.955 24(13)	0.966 9(5)	0.949 54(11)	1.158 4(3)	1.111 9(3)
c / nm	2.006 0(4)	2.001 2(3)	2.040 8(11)	2.009 2(2)	0.972 7(3)	1.395 0(3)
α / (°)	90	90	90	90	90	69.788(3)
β / (°)	122.638(2)	122.815(2)	122.874(6)	123.06(10)	113.816(3)	76.132(3)
γ / (°)	90	90	90	90	90	87.981(3)
V / nm^3	4.200 2(14)	4.141 6(11)	4.331(4)	4.117 4(8)	2.102 6(10)	1.098 8(4)
Z	8	8	8	8	4	2
D_c / ($g\cdot cm^{-3}$)	1.943	1.978	1.915	2.031	1.958	1.915
F(000)	2 400.0	2 408.0	2 432.0	2 440.0	1 200	616
R_{int}	0.023	0.022 9	0.017 4	0.020 4	0.029 2	0.023 5
GOF on F^2	1.081	1.016	1.061	1.015	0.996	0.986
R_1[a] ($I>2\sigma(I)$)	0.031 7	0.029 2	0.030 0	0.028 1	0.033 4	0.027 2
wR_2[b] (all data)	0.108 9	0.116 6	0.122 2	0.117 1	0.122 6	0.105 7

[a] $R_1=\sum||F_o|-|F_c||/\sum|F_o|$; $wR_2=[\sum w(F_o^2-F_c^2)^2/\sum w(F_o^2)^2]^{1/2}$.

Table 2 Selected bond lengths (nm) of 1~6

			1		
Pr1-O6^{i}	0.238 6(3)	Pr1-O5	0.246 5(3)	Pr1-O8	0.255 2(3)
Pr1-O3	0.241 3(3)	Pr1-O1	0.247 7(3)	Pr1-O7	0.260 9(3)
Pr1-O2^{ii}	0.243 6(3)	Pr1-O4^{ii}	0.249 9(3)		
			2		
Nd1-O5^{ii}	0.236 7(2)	Nd1-O6	0.244 5(2)	Nd1-O7	0.252 4(3)
Nd1-O2^{iii}	0.239 5(2)	Nd1-O4^{iii}	0.245 8(3)	Nd1-O8	0.258 1(2)
Nd1-O3	0.240 9(3)	Nd1-O1	0.248 0(2)		
			3		
Eu1-O1	0.236 0(3)	Eu1-O2^{i}	0.243 8(3)	Eu1-O7	0.254 3(3)
Eu1-O5	0.239 3(3)	Eu1-O4^{ii}	0.245 3(3)	Eu1-O8	0.259 8(3)
Eu1-O3	0.239 9(3)	Eu1-O6^{ii}	0.247 5(3)		
			4		
Gd1-O3	0.231 9(3)	Gd1-O4^{ii}	0.239 9(3)	Gd1-O7	0.248 5(3)
Gd1-O1	0.234 9(2)	Gd1-O6^{i}	0.240 3(3)	Gd1-O8	0.254 2(3)
Gd1-O5	0.234 9(3)	Gd1-O2^{i}	0.242 2(2)		
			5		
Dy1-O4^{ii}	0.226 6(5)	Dy1-O3^{i}	0.239 4(4)	Dy1-O1	0.243 8(4)
Dy1-O4^{iii}	0.226 6(5)	Dy1-O7^{i}	0.239 6(5)	Dy1-O1^{i}	0.243 8(4)
Dy1-O3	0.239 4(4)	Dy1-O7	0.239 6(5)		
			6		
Gd1-O9^{i}	0.224 46(18)	Gd1-O4^{ii}	0.238 3(2)	Gd1-N2	0.257 7(2)
Gd1-O9	0.227 41(18)	Gd1-O2^{i}	0.241 3(3)	Gd1-N1	0.258 6(3)
Gd1-O3	0.236 2(2)	Gd1-O1	0.242 0(2)		

Symmetry codes: **1**: ^{i} $-x$, $-y+2$, $-z+1$; ^{ii} $-x$, $-y+1$, $-z+1$; **2**: ^{ii} $-x+2$, $-y+2$, $-z+2$; ^{iii} $-x+2$, $-y+1$, $-z+2$; **3**: ^{i} $-x+2$, $-y+1$, $-z$; ^{ii} $-x+2$, $-y+2$, $-z$; **4**: ^{i} $-x+2$, $-y+1$, $-z+1$; ^{ii} $-x+2$, $-y+2$, $-z+1$; **5**: ^{i} $2-x$, y, $1.5-z$; ^{ii} x, $2-y$, $0.5+z$; ^{iii} $2-x$, $2-y$, $1-z$; **6**: ^{i} $-x+1$, $-y+1$, $-z+1$; ^{ii} $-x$, $-y+1$, $-z+1$.

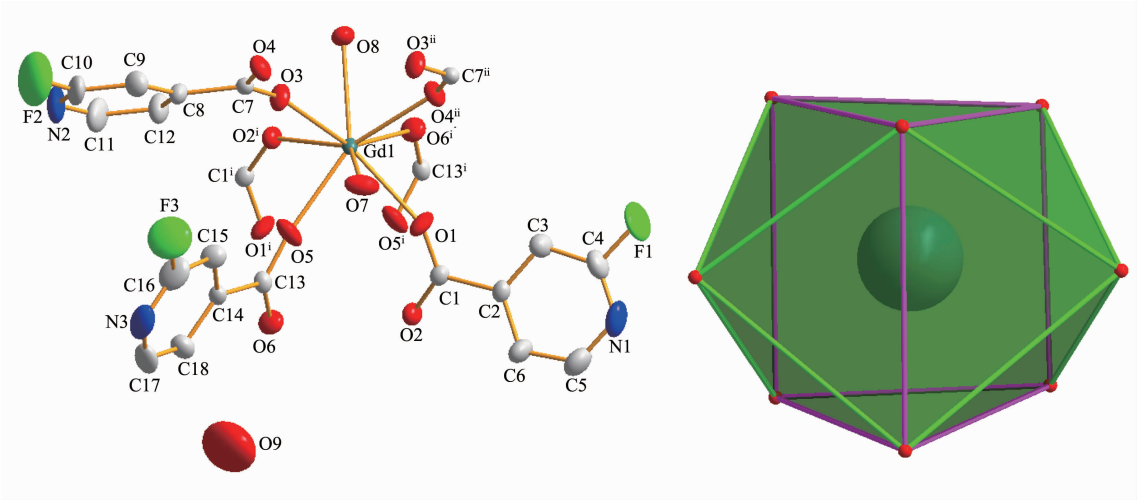

Hydrogen atoms are omitted for clarity; ^{i} $2-x$, $1-y$, $1-z$; ^{ii} $2-x$, $2-y$, $1-z$

Fig.1 Coordination environment with thermal ellipsoids shown at 30% probability and polyhedron of compound **4**

atom is close to bi-capped triangular-prisms that is six O atoms from different $FINA^{-}$ anions (O1, O2^{i}, O3, O4^{ii}, O5, O6^{i}) form the body of prism, while other two O atoms (O7 and O8) from coordinated H_2O molecule occupy the capped positions. The Gd-O distances range from 0.231 9(3) to 0.254 2(3) nm, and the O-

Gd-O bond angles are in the range from 69.48(10)° to 145.42(10)°. All of the ligands are bridging-bidentate coordination mode with the carboxylate group in a η^1:η^1-μ_2 bridging mode (Fig.2). The pyridyl group is not involved in the coordination because of the influence of fluorine atoms. Adjacent Gd centers are bridged by carboxylates in quadruple and dual modes alternately to form one-dimensional (1D) helical chains along the *b*-axis (Fig2). The distance between Gd atoms is 0.443 73(5) and 0.520 23(6) nm, respectively. All of helical chains are further extended via the intermolecular $\pi\cdots\pi$ interactions, C–H⋯F hydrogen bonds (the distance of C⋯F is 0.327 43(5) nm) and strong O–H⋯N hydrogen bonds into a 3D supramolecular structure (Fig.3). Interestingly, there is a small 1D solvent channel along the *b*-axis, constructed by two neighboring chains along the *c* axis, where water molecules are located and interact with the main

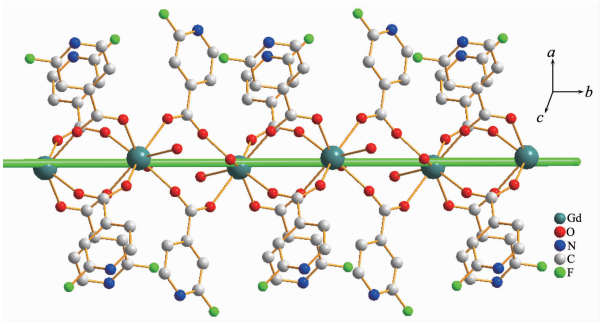

Hydrogen atoms and the solvent water molecule are omitted for clarity

Fig.2　One-dimensional helix chain of compound **4** along the *b* axis

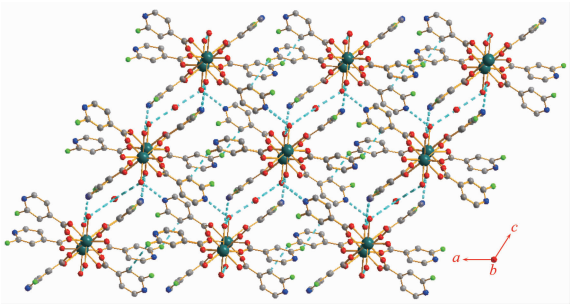

Gd: dark green, C: gray, N: blue, O: red, F: green

Fig.3　Packing diagram of **4** in a view along the *b* axis

structure via the intermolecular strong O–H ⋯ O hydrogen bonds.

Crystal structure of **5**: Compound **5** was synthesized by the same method as **1**~**4** and also crystallizes in the monoclinic crystal system, *C*2/*c* space group but the structure is different to **1**~**4** may be because of the lanthanide contraction effect, which has been found in other reported[7,28]. The asymmetric unit of **5** contains one crystallographically independent Dy^{3+} cation, three $FINA^-$ ligands and two coordinated waters (Fig.4). Dy center adopts distorted dodecahedron geometry with six oxygen donors from five carboxylate groups (O1, O1^{i}, O3, O3^{i}, O4^{ii}, O4^{iii}) and two (O7, O7^{i}) from coordinated water molecules. The Dy-O distances range from 2.266(5) to 0.243 8(4) nm, and the O-Dy-O bond angles are in the range from 52.9(2)° to 155.2(3)°. Carboxylate groups of the $FINA^-$ ligands adopt different coordination modes: one of the carboxylate groups in a bridging-bidentate (η^1:η^1-μ_2)

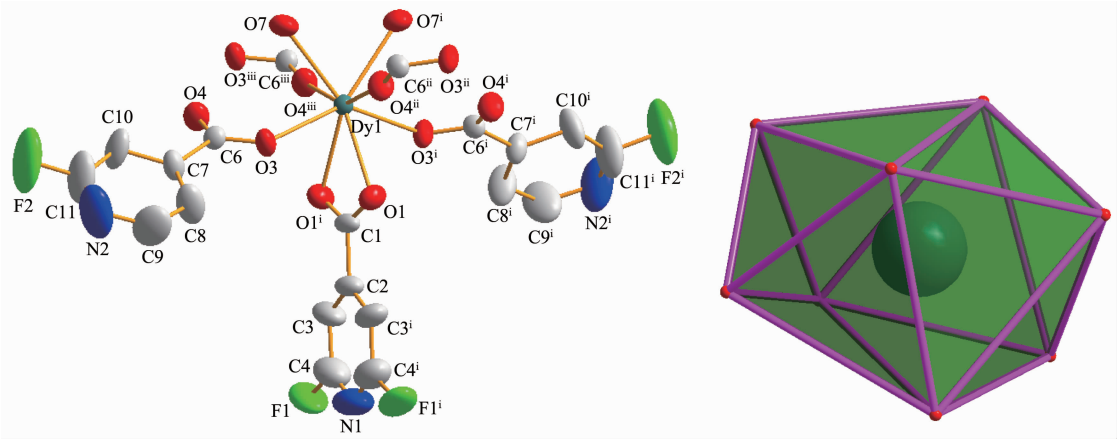

Hydrogen atoms are omitted for clarity; [i] 2–*x*, *y*, 1.5–*z*; [ii] *x*, 2–*y*, 0.5+*z*; [iii] 2–*x*, 2–*y*, 1–*z*

Fig.4　Coordination environment with thermal ellipsoids shown at 30% probability and polyhedron of compound **5**

coordination mode, while the other one shows a chelating bidentate coordination mode. Adjacent Dy centers are bridged by two carboxylates to form one-dimensional (1D) helical chains along the *c*-axis (Fig. 5). The helical chains are further extended via the intermolecular O–H ··· N hydrogen bonds between coordinated water molecule to pyridyl group into a 3D supramolecular structure.

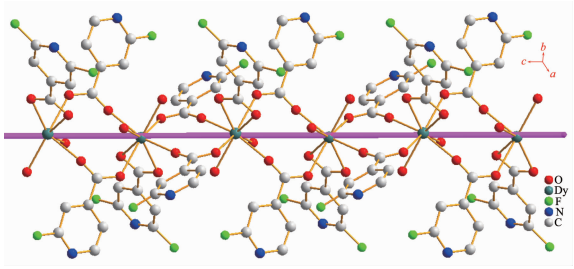

Hydrogen atoms and the solvent water molecule are omitted for clarity

Fig.5 One-dimensional helix chain of compound **5** along the *c* axis

Crystal structure of **6**: Unlike **1**~**5**, compound **6** is synthesized under solvothermal conditions and crystallizes in the triclinic crystal system, $P\bar{1}$ space group. The asymmetric unit of **6** contains one crystallographically independent Gd^{3+} cation, two FINA ligands and one hydroxy group. Gd center also adopts distorted dodecahedron geometry with four oxygen donors from different carboxylate groups (O1, $O2^{i}$, O3, $O4^{ii}$), two oxygen donors (O9, $O9^{i}$) from two hydroxyl groups and two nitrogen donors from one 1,10-phenthroline molecule (Fig.6). The bond lengths around Gd center are given in Table 2. Carboxylate groups of the $FINA^-$ ligands adopt the same coordination modes as they are in **1**~**4**, that is a bridging-bidentate (η^1:η^1-μ_2) coordination mode. Adjacent Gd centers are bridged by two carboxylates and two μ_2-OH groups to form a dinuclear SBU with a metal··· metal distance about 0.363 98(7) nm and two phen molecules coordinated to two Gd centers in the opposite position, the two $FINA^-$ ligands are coplanar to each other and the plane is almost perpendicular to the plane of Gd_2O_2 constructed by Gd centers and the hydroxy groups in the SBU. The dinuclear units are then bridged by other two carboxylates to form 1D helix chain along the a-axis with the distance between adjacent Gd atoms about 0.524 51(10) nm (Fig.7. The chains are further extended into a 3D supramolecular structure via the intermolecular C–H ··· N hydrogen bonds (the distance of C···N is 0.336 8(5) nm) and C–H ··· F hydrogen bonds (the distance of C ··· F is 0.327 43(5) nm) between phen rings to pyridyl groups and the $\pi \cdots \pi$ interactions (the shortest distance between two pyridyl rings is about 0.335 82(6) nm) (Fig.8).

2.2 PXRD and thermogravimetric analysis (TGA)

X-ray powder diffraction (XRPD) was used to check the purity of compounds **1**~**6**. As shown in Fig.

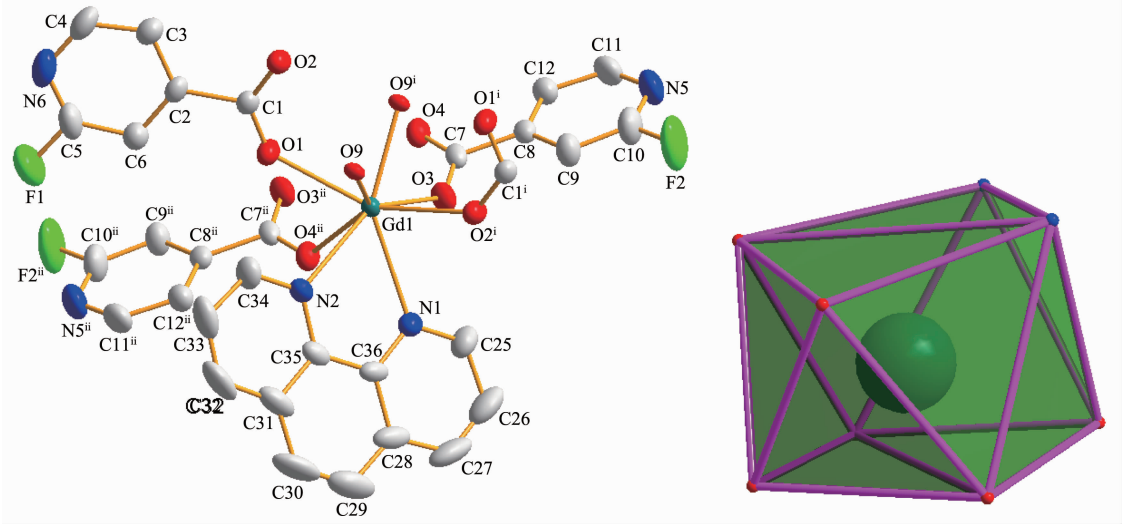

Hydrogen atoms are omitted for clarity; [i] 1–*x*, 1–*y*, 1–*z*; [ii] –*x*, 1–*y*, 1–*z*

Fig.6 Coordination environment with thermal ellipsoids shown at 30% probability and polyhedron of compound **6**

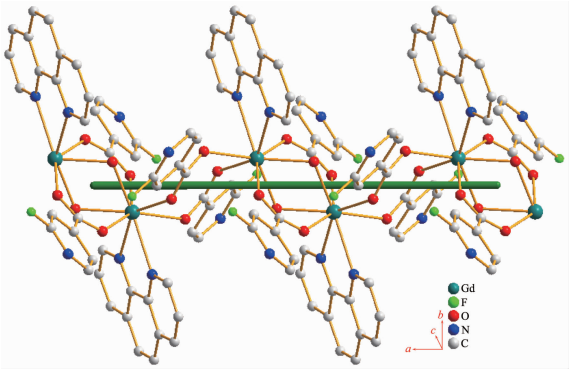

Hydrogen atoms are omitted for clarity

Fig.7　One-dimensional helix chain along the *a* axis of compound **6**

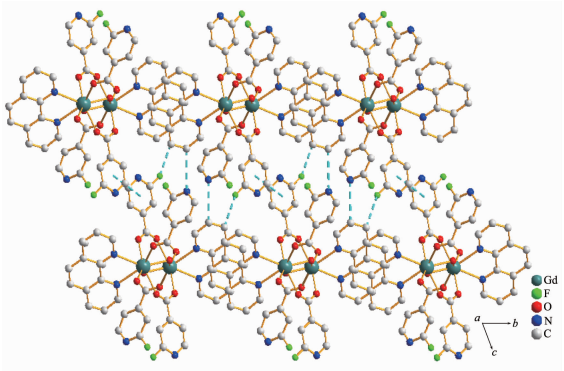

Gd: dark green, C: gray, N: blue, O: red, F: green

Fig.8　Packing diagram of **6** in a view along the *a* axis

9, the experimental XRPD patterns match well with the simulated based on the single crystal structure analysis. The result proves the phase purity of the bulk samples of compounds **1**~**6**, together with the result of the elemental analyses. Thermal analyses for **1**~**6** were carried out from room temperature to 900 ℃ under a nitrogen atmosphere and the TGA diagrams are shown in Fig.10. For compound **1**~**5**, the weight loss of two coordinated and one lattice water (except **5**) molecules is in the range of 82~143 ℃ for **1** (Observed, 8.08%; Calculated, 8.78%), 89~163°C for **2** (Observed, 8.06%; Calculated, 8.73%), 133~181 ℃ for **3** (Observed, 7.59%; Calculated, 8.62%), 84~164 ℃ for **4** (Observed, 7.66%; Calculated, 8.55%), and 106~166 ℃ for **5** (Observed, 5.86%; Calculated, 5.82%), respectively. Further weight loss until about 278 ℃ for **1**, 266 ℃ for **2**, 297 ℃ for **3**, 278 ℃ for **4**, 301 ℃ for **5**, suggests the decomposition of the framework of these compounds. The TGA curve of **6** shows that no obvious weight loss is observed until the decomposition of the framework occurs at about 320 ℃.

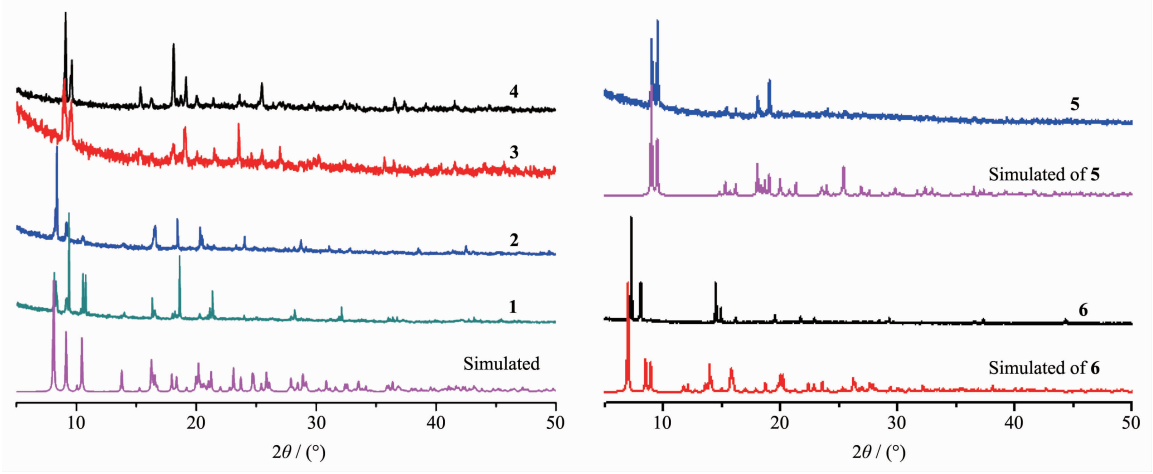

Fig.9　PXRD patterns of the simulation based on the single-crystal analysis and as-synthesized sample of **1**~**6**

2.3　Photoluminescent properties

The solid state luminescent properties of free FINA ligand, compounds **3**, and **4** were investigated at room temperature. As shown in Fig.11, the emission spectrum of free FINA ligand gives an emission peak at 383 nm (λ_{Ex}=330 nm), which is attributed to the $\pi^* \rightarrow \pi$ transitions. Upon excitation at 394 nm (the maximum of the solid-state excitation spectrum (Fig. 11, inset)), compound **3** shows the characteristic emission bands of the Eu^{3+} ion centered at 592, 618, 654, and 698 nm which can be attributed to the $^5D_0 \rightarrow {}^7F_J$ (J=1~4) transitions, respectively[4,29-31]. Note that the $^5D_0 \rightarrow {}^7F_2$ (electric-dipole which is hypersensitive to the coordination environment of the Eu^{3+} ion) transition at

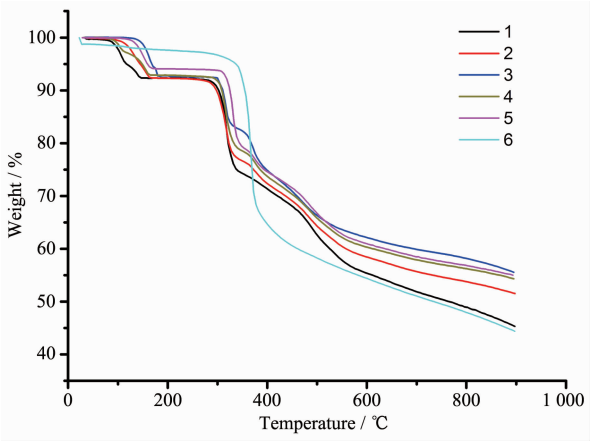

Fig.10 TGA plots of the samples of **1~6**

618 nm for **3** dominates the whole emission spectrum. Moreover, the ligand-centered emission is quenched in the spectra of **3**, which suggest that the ligand is suitable for the sensitization of red luminescence for Eu^{3+} ion[32-33]. The intensity of the $^5D_0 \rightarrow {}^7F_2$ transition is about 6 times stronger than that of the $^5D_0 \rightarrow {}^7F_1$ transition (magnetic dipole, which is fairly insensitive to the environment of the Eu^{3+} ion), suggesting that the coordination environment of the Eu^{3+} ion is low-symmetric[34-35], which is agreement with the results from structural analyses. The luminescent lifetime of **3** has also been measured at room temperature. The decay is well fitted with a monoexponential function and yields a lifetime of 333.81 μs (determined by monitoring $^5D_0 \rightarrow {}^7F_2$ line excited at 394 nm), implying that all the Eu^{3+} sites experience similar decay rates[32], which is consistent with the crystallographic observation that the same Eu center in the structure.

For **4**, there is a broad emission band at about 402 nm under the excitation of 342 nm (Fig.11). Because of no characteristic emission of Gd center, and by comparing with the luminescence behavior of the free ligand, we can draw a conclusion that the emissions for compounds **4** may be due to the intramolecular $\pi \rightarrow \pi^*$ transition of ligands.

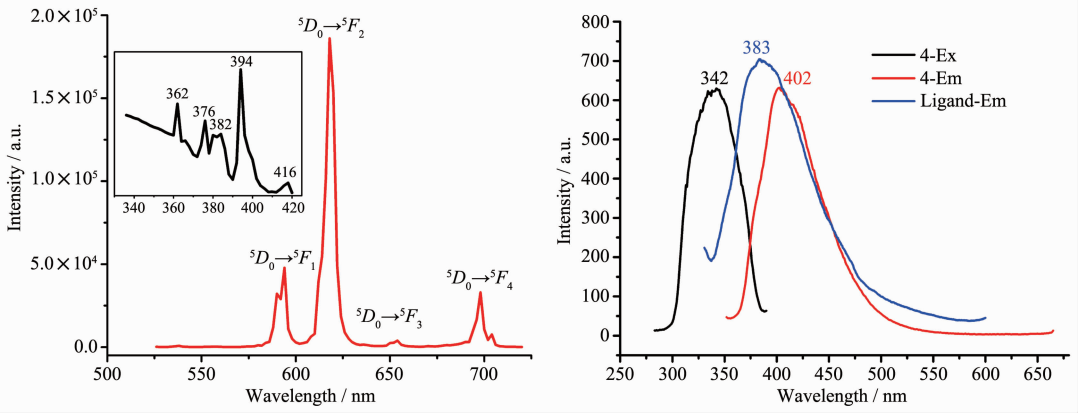

Fig.11 (left) Solid state excitation and photo emission spectra of **3**, (right) **4** and HL (λ_{Ex}=330 nm) in solid state at room temperature

2.4 Magnetic properties

The temperature dependencies of the magnetic susceptibilities in the form of $\chi_M T$ and χ_M vs T for compounds **2~6** are given in Fig.12. The $\chi_M T$ product of **2** at 300 K is 1.72 $cm^3 \cdot K \cdot mol^{-1}$, which is more than the expected value of 1.64 $cm^3 \cdot K \cdot mol^{-1}$ for a non-interacting Nd^{3+} ion in the $^4I_{9/2}$ ground state[2,36]. As the temperature is lowered, $\chi_M T$ decreases more and more rapidly within the entire temperature range and reaches 0.43 $cm^3 \cdot K \cdot mol^{-1}$ at 1.9 K. This indicates the presence of possible antiferromagnetic interactions between the adjacent Nd^{3+} cations. To obtain a rough quantitative estimation of the magnetic interaction between Nd^{3+} ions, the susceptibility data were fitted according to eq 1in the temperature range of 50~300 K[2,37].

$$\chi_{Nd}=\frac{Ng^2\beta^2}{4kT}[81e^{-81\Delta/(4kT)}+49e^{-49\Delta/(4kT)}+25e^{-25\Delta/(4kT)}+9e^{-9\Delta/(4kT)}+e^{-\Delta/(4kT)}]/[e^{-81\Delta/(4kT)}+e^{-49\Delta/(4kT)}+e^{-25\Delta/(4kT)}+e^{-9\Delta/(4kT)}+e^{-\Delta/(4kT)}] \quad (1)$$

In eq **1**, Δ is the zero-field splitting parameter, N is Avogadro's number, β is the Bohr magneton, and k

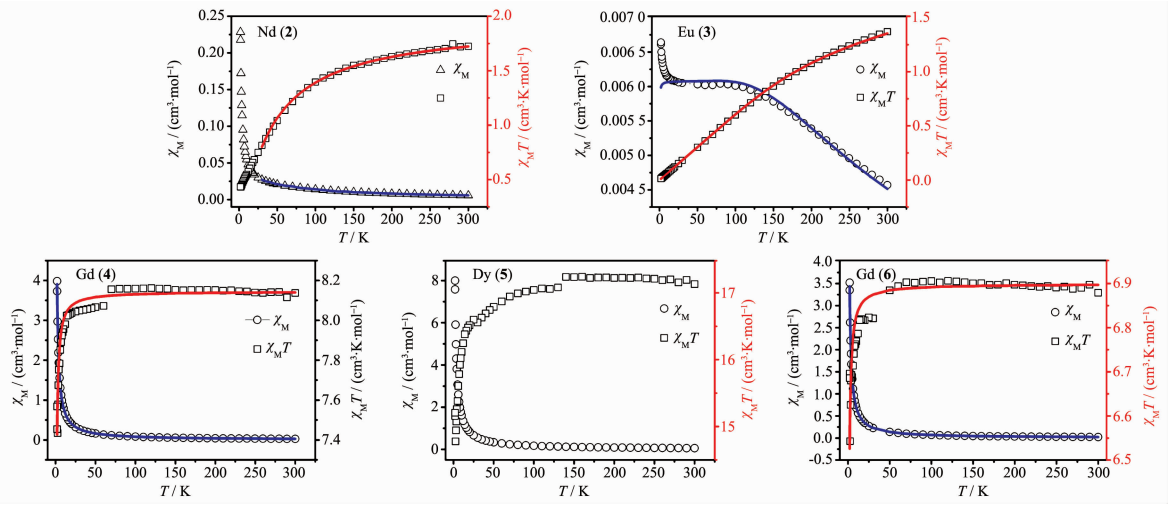

Fig.12　Plots of $\chi_M T$ and χ_M vs T for compounds **2~6**

is the Boltzmann constant. The zJ' parameter based on the molecular field approximation in eq **2** is introduced to simulate the magnetic interaction between the Nd^{3+} ions[37].

$$\chi=\chi_{Nd}/[1-[2zJ'/(Ng^2\beta^2)]\chi_{Nd}] \quad (2)$$

The least-squares analysis of the magnetic data gives $\Delta=-1.57$ cm^{-1}, $g=0.79$, $zJ'=-2.25$ cm^{-1}, with an agreement factor R ($\sum[(\chi_M T)_{obsd}-(\chi_M T)_{calcd})]^2/\sum[(\chi_M T)_{obsd}]^2$) of 6.12×10^{-5}. The negative value of zJ' confirms that antiferromagnetic interactions between Nd^{3+} ions.

For **3**, the $\chi_M T$ product of 1.37 cm^3·K·mol^{-1} at room temperature is smaller than the expected value of 1.53 cm^3·K·mol^{-1} for the excited states of one free Eu^{3+} ion[29,38]. As the temperature cooling down, the $\chi_M T$ values decrease steeply to 0.012 cm^3·K·mol^{-1} at 1.9 K, which is close to the expected value of its ground state. The shape of these curves is a typical characteristic occurrence of thermally populated excited states, and the magnetic susceptibility can be fitted with eq **3**[39].

$$\chi_{Eu}=\frac{N\beta^2}{3kx(T-\theta)}[24+(27x/2-3/2)e^{-x}+(135x/2-5/2)e^{-3x}+(189x-7/2)e^{-6x}+(405x-9/2)e^{-10x}+(1\ 485x/2-11/2)e^{-15x}+(2457x/2-13/2)e^{-21x}]/[1+3e^{-x}+5e^{-3x}+7e^{-6x}+9e^{-10x}+11e^{-15x}+13e^{-21x}] \quad (3)$$

In this expression, $x=\lambda/(kT)$ (λ is the spin-orbit coupling parameter) and the Weiss constant θ accounts for the magnetic interactions between neighboring Eu^{3+} ions. The best fitting results are $\lambda=343$ cm^{-1}, $\theta=-0.03$ K, and $R=5.9\times10^{-5}$. The value of λ is close to previous reported[39]. The negative θ value confirms the presence of very weak antiferromagnetic interactions between Eu^{3+} ions.

For **4** and **6**, The SQUID measurement shows a $\chi_M T$ value at room temperature of 8.14 cm^3·K·mol^{-1} to **4**, which is somewhat larger than the theoretical value of 7.88 cm^3·K·mol^{-1}, the expected value for a magnetically isolated Gd^{3+} ion with $S=7/2$, $g=2.0$. While the value of $\chi_M T$ at 300 K for **6** is 6.88 cm^3·K·mol^{-1}, which is obviously smaller than the theoretical value but similar to previously reported[36]. The shape of the curves for **4** and **6** is almost same. Upon cooling the sample, the value practically remains constant until 70 K for **4** and 50 K for **6** after which decreases abruptly to 7.43 cm^3·K·mol^{-1} for **4** and 6.54 cm^3·K·mol^{-1} for **6** at 2.5 K. This behaviour is indicative of the existence of weak antiferromagnetic interactions between the Gd^{3+} ions and the experimental data were fit using the equation of 1D chain (eq **4**)[40].

$$\chi=[Ng^2\beta^2/(3kT)]S(S+1)(1+u)/(1-u) \quad (4)$$

In the expression, u is the Langevin function, defined in eq **5**.

$$u=\coth[JS(S+1)/kT]-kT/[JS(S+1)] \quad (5)$$

The best fit gives parameters $g=2.034$, $J=-0.012$ cm^{-1}, $R=3.7\times10^{-5}$ for **4** and $g=1.872$, $J=-0.007$ cm^{-1}, $R=4.4\times10^{-5}$ for **6**. The negetive J value confirms the very weak antiferromagnetic interactions between Gd^{3+} ions in the two compounds.

For **5**, the $\chi_M T$ value at room temperature is 17.13 $cm^3 \cdot K \cdot mol^{-1}$, which is more than the expected value of 14.17 $cm^3 \cdot K \cdot mol^{-1}$ for one magnetically isolated Dy^{3+} ion[6,36]. The shape of the curves for **5** is similar to **4** and **6** indicating the presence of possible weak antiferromagnetic interactions within the polymer. The temperature dependence of the reciprocal susceptibilities ($1/\chi_M$) obeys the Curie-Weiss law [$\chi_M = C/(T-\theta)$], Weiss constant $\theta = -1.0$ K, and Curie constant $C = 14.0$ $cm^3 \cdot K \cdot mol^{-1}$ in the whole temperature range. This result confirms the antiferromagnetic interactions between Dy^{3+} ions.

3 Conclusions

In summary, six new 1D helical LnPCs based on 2-fluoroisonicotinic acid were synthesized for the first time, and their structures and properties have been explored. Because of the lanthanide contraction effect, the ligands of **1~4** and **5** exhibit different coordination modes and lead to different structures. Interestingly, there is a small 1D solvent channel in **1~4**. Compound **3** exhibits intense red luminescence of the Eu^{3+} ion with a long decay lifetime in the solid state at room temperature, while **4** shows the intraligand fluorescence, because its emission spectrum is similar to the free ligand. The antiferromagnetic behavior of compounds **2~6** has been discussed.

References:

[1] Yamada T, Otsubo K, Makiura R, et al. *Chem. Soc. Rev.*, **2013**,**42**(16):6655-6669

[2] Feng X, Wang J, Liu B, et al. *Cryst. Growth Des.*, **2011**,**12**(2):927-938

[3] QIU Yan-Nan(仇衍楠), SUN Li-Ning(孙丽宁), LIU Tao(刘涛), et al. *J. Chinese Soc. Rare Earths*(中国稀土学报), **2012**, **30**(2):129-145

[4] Han Y, Li X, Li L, et al. *Inorg. Chem.*, **2010**,**49**(23):10781-10787

[5] Zhou Q, Yang F, Xin B, et al. *Chem. Commun.*, **2013**,**49**(74):8244-8246

[6] Lin S Y, Zhao L, Ke H, et al. *Dalton Trans.*, **2012**,**41**(11):3248-3252

[7] Zhao X Q, Liu X H, Zhao B. *Dalton Trans.*, **2013**,**42**(41):14786-14793

[8] Höller C J, Matthes P R, Adlung M, et al. *Eur. J. Inorg. Chem.*, **2012**,**33**:5479-5484

[9] Allendorf M D, Bauer C A, Bhakta R K, et al. *Chem. Soc. Rev.*, **2009**,**38**(5):1330-1352

[10]Reddy M L, Sivakumar S. *Dalton Trans.*, **2013**,**42**(8):2663-2678

[11]Zhang Z H, Chen S C, He M Y, et al. *Cryst. Growth Des.*, **2013**,**13**(3):996-1001

[12]Wu Y P, Li D S, Fu F, et al. *Polyhedron*, **2012**,**31**(1):188-195

[13]Hulvey Z, Furman J D, Turner S A, et al. *Cryst. Growth Des.*, **2010**,**10**(5):2041-2043

[14]Fischer R A, Wll C. *Angew. Chem. Int. Ed.*, **2008**,**47**(43):8164-8168

[15]Yang C, Wang X, Omary M A. *Angew. Chem. Int. Ed.*, **2009**, **48**(14):2500-2505

[16]Zhang Z H, Chen S C, He M Y, et al. *Cryst. Growth Des.*, **2011**,**11**(12):5171-5175

[17]Serre C. *Angew. Chem. Int. Ed. Engl.*, **2012**,**51**(25):6048-6050

[18]Seidel C, Ahlers R, Ruschewitz U. *Cryst. Growth Des.*, **2011**, **11**(11):5053-5063

[19]Pachfule P, Das R, Poddar P, et al. *Inorg. Chem.*, **2011**,**50**(9):3855-65

[20]Fernandez C A, Thallapally P K, Motkuri R K, et al. *Cryst. Growth Des.*, **2010**,**10**(3):1037-1039

[21]Chen T H, Popov I, Zenasni O, et al. *Chem. Commun.*, **2013**, **49**(61):6846-6848

[22]Altomare A C G, Giacovazzo C, Guagliardi A, et al. *J. Appl. Crystallogr.*, **1994**,**27**:435-436

[23]Sheldrick G M, Schneider T R. *Macromolecular Crystallogr. B*, **1997**:319-343

[24]Sheldrick G M. *Acta Crystallogr. A*, **2008**,**64**:112-122

[25]Farrugia L. *J. Appl. Crystallogr.*, **1999**,**32**:837-838

[26]Xu Z, Mitzi D B. *Chem. Mater.*, **2003**,**15**(19):3632-3637

[27]Lancaster S J, Mountford A J, Hughes D L, et al. *J. Organometallic Chem.*, **2003**,**680**:193-205

[28]ZHUANG Wen-Juan(庄文娟), ZHENG Xiang-Jun(郑向军), SUN Hao-Ling(孙豪岭), et al. *Chinese J. Inorg. Chem.*(无机化学学报), **2008**,**24**(8):1305-1310

[29]Xu J, Su W, Hong M. *Cryst. Growth Des.*, **2010**,**11**(1):337-346

[30]Hou Y L, Xiong G, Shen B, et al. *Dalton Trans.*, **2013**,**42**(10):3587-3596

[31]LIU Jian-Feng(刘建风), CHEN Ji-Fei(陈吉妃), ZHAO Guo-Liang(赵国良). *Chinese J. Inorg. Chem.*(无机化学学报), **2011**,**27**(1):100-106

[32]Yan L, Yue Q, Jia Q X, et al. *Cryst. Growth Des.*, **2009**,**9**(7):2984-2987

[33]Zhang Y H, Li X, Song S. *Chem. Commun.*, **2013**,**49**(88):10397-10399

[34]Zhang S R, Du D Y, Tan K, et al. *Chem. Eur. J.*, **2013**,**19**(34):11279-11286

[35]Sun J K, Cai L X, Chen Y J, et al. *Chem. Commun.*, **2011**, **47**(24):6870-6872

[36]Wang Y L, Jiang Y L, Xiahou Z J, et al. *Dalton Trans.*, **2012**,**41**(37):11428-11437

[37]Feng X, Ling X L, Liu L, et al. *Dalton Trans.*, **2013**,**42**(28):10292-10303

[38]Sun M L, Zhang J, Lin Q P, et al. *Inorg. Chem.*, **2010**,**49**(20):9257-9264

[39]Ji B, Deng D, He X, et al. *Inorg. Chem.*, **2012**,**51**(4):2170-2177

[40]Caadillas-Delgado L, Martín T, Fabelo O, et al. *Chem. Eur. J.*, **2010**,**16**(13):4037-4047